energies

MDPI

Article

High-Fidelity Aeroelastic Analysis of a Wind Turbine Using a Nonlinear Frequency-Domain Solution Method

Shine Win Naung [1,*], Mohammad Rahmati [2] and Htet Shine [3]

[1] School of Engineering, University of the West of England, Bristol BS16 1QY, UK
[2] Department of Mechanical and Construction Engineering, Northumbria University, Newcastle upon Tyne NE1 8ST, UK; mohammad.rahmati@northumbria.ac.uk
[3] Energy Department, Capula Ltd., Stone ST15 0LT, UK; htet.shine@capula.com
* Correspondence: Shine.WinNaung@uwe.ac.uk

Abstract: This paper investigates the aeroelastic behaviour of a full wind turbine model with realistic blade vibration amplitude (9% span) using a nonlinear frequency-domain solution method. The primary objective is to demonstrate the computational efficiency of this method for an aeroelastic analysis compared to resource-intensive time-domain approaches. The underlying CFD model was validated against experimental data and benchmark simulations. The frequency-domain method was then validated against a conventional time-domain method, comparing aerodynamic damping and unsteady pressure distributions, with strong agreement observed. Results show a more complex unsteady pressure distribution at 324.5 RPM compared to 424.5 RPM, directly affecting aerodynamic damping. While aeroelastic stability was observed at both speeds, aerodynamic damping was significantly lower at 324.5 RPM. Flow field analysis reveals a clear relationship between relative velocity, static pressure, and blade vibration. Critically, the frequency-domain method achieved comparable accuracy to the time-domain method but with a significantly reduced computational cost (9 h versus 120 h), making it highly attractive for routine aeroelastic analyses and design optimisation.

Keywords: wind turbines; renewable energy; aerodynamics; aeroelasticity; computational fluid dynamics; fluid–structure interaction

Academic Editor: Ahmed Abu-Siada

Received: 2 February 2025
Revised: 22 February 2025
Accepted: 23 February 2025
Published: 28 February 2025

Citation: Win Naung, S.; Rahmati, M.; Shine, H. High-Fidelity Aeroelastic Analysis of a Wind Turbine Using a Nonlinear Frequency-Domain Solution Method. *Energies* **2025**, *18*, 1195. https://doi.org/10.3390/en18051195

1. Introduction

The transition to a 100% decarbonised electricity system is crucial for the UK, as set out by the government's ten-point plan, which aims for net-zero greenhouse gas emissions by 2050 [1]. Wind power plays a vital role in this transformation, and the UK's ambition to double onshore wind and quadruple offshore wind by 2030 [2]. This global trend is evidenced by the Global Wind Report 2024, which revealed a record 117 GW of new wind capacity installed worldwide in 2023; however, the world still needs to accelerate wind energy installations to approximately 320 GW annually. Continuous research and development in wind energy technologies led to an increase in the sizes of wind turbines, with the largest wind turbine to date reaching 260 m in rotor diameter [3]. While large rotor diameters produce more electricity, they can also potentially introduce aeroelastic instabilities including flutter and vortex-induced vibration [4].

Numerical modelling and simulation are crucial for advancing wind power research, particularly given the challenges of conducting experiments on large-scale turbines [5]. The Blade Element Momentum (BEM) method [6] remains a widely used tool in wind turbine design and optimisation to provide reasonable results without excessive computational

demands, based on sufficient aerofoil data. While computationally efficient and commonly employed for predicting aerodynamic loads [7,8], the BEM method typically relies on quasi-steady assumptions and empirical corrections to account for tip loss, dynamic inflow, and stall [9,10]. Consequently, it is often considered a low-fidelity model, primarily suited for the initial design stages of modern wind turbines due to its inability to resolve detailed flow structures [11].

Vortex models offer advantages over the BEM method by providing a better understanding of wake development and flow structures around wind turbines. Lee et al. [12] developed an unsteady vortex-lattice method for the wake analysis, while Rodriguez et al. [13,14] employed a free-wake method for the aeroelastic modelling of offshore wind turbines. Breton et al. [15] explored a prescribed-wake method for similar analyses. However, a typical key limitation of most vortex models is their simplifications of viscous effects.

Actuator-type methods, such as the works of Refs [16,17], offer another approach to the aerodynamic analysis of wind turbines. These methods represent a rotor or blade as a disk (actuator disk method) or line (actuator line method) with varying load distributions. While conceptually similar to the BEM method in calculating aerodynamic loads, actuator-type methods are typically coupled with a flow solver, such as the Navier–Stokes equations, to analyse wake development. Sørensen et al. [18] employed an actuator disk method with a finite difference Navier–Stokes solver for unsteady wind turbine simulations. Troldborg et al. [19] used an actuator line method to study wind turbines operating in unsteady turbulent wakes. Although actuator-type models provide valuable insights into turbulent wake structures and reasonably accurate loading predictions, these methods, similar to the BEM models, require sufficient aerofoil data. Furthermore, the inclusion of a flow solver makes them significantly more computationally expensive than BEM methods, as discussed in [20].

Computational Fluid Dynamics (CFD) methods, often termed "high-fidelity" approaches, solve the Navier–Stokes equations and, with appropriate turbulence modelling, can not only compute aerodynamic loads but also resolve detailed flow structures. Liu et al. [21] developed a fully coupled CFD method for the analysis of floating offshore wind turbine aerodynamics. CFD is frequently coupled with structural models such as Finite Element Analysis (FEA) methods or Computational Structural Dynamics (CSD) methods for the aeroelastic analyses of wind turbines, as demonstrated by Wang et al. [22], and Dose et al. [23,24]. The primary disadvantage of CFD-based methods lies in their substantial computational cost and resource requirements, particularly for fully unsteady simulations.

The development of efficient numerical tools that balance accuracy with reduced computational cost has become a key focus in the fields of aerodynamics and aeroelasticity, including wind turbines. Frequency-domain methods, such as the harmonic solution approach explored by Rahmati et al. [25], have emerged as promising solutions for aeroelasticity modelling. Win Naung et al. [26] recently introduced a nonlinear frequency-domain method for wind turbine aerodynamic and aeroelastic analysis, incorporating different sources of flow unsteadiness such as inflow wake and turbulence, blade vibration, and rotor–tower interaction.

From the literature review conducted, it is clear that the computational resources and costs are the main challenges for the aeroelastic modelling of turbomachinery including wind turbines. It is also highlighted that the frequency-domain methods are highly efficient and innovative by reducing the computational costs significantly without compromising the required accuracy, compared to traditional time-domain CFD methods. This paper aims to address the computational challenges associated with the aeroelastic analysis of wind turbines by demonstrating the effectiveness of a nonlinear frequency-domain solution method. Aeroelastic analyses of a wind turbine with a relatively large amplitude

blade structural oscillation at different rotational speeds are performed using the nonlinear frequency-domain method in this paper. The results obtained from the frequency-domain solution method are compared to that of the time-domain method to validate the reliability of the method. This paper is built on the authors' previous works [26] by exploring a complete wind turbine model with a realistic and large amplitude of blade structural oscillation at different rotational speeds.

The paper is structured as follows. Section 2 presents the physical description of the wind turbine used in this study, followed by Methodologies in Section 3, which includes computational domain and grid, numerical methods employed and validation. Section 4 (Results and Discussion) discusses the results obtained from this study, and Section 5 concludes the overall findings of the paper.

2. Physical Description

The numerical modelling focuses on the MEXICO (Model Rotor Experiment in Controlled Conditions) wind turbine model, a recognised benchmark model, in wind turbine aerodynamic studies. This three-bladed rotor has a 4.5 m diameter, with each blade measuring 2.04 m in length. Simulations are performed at a wind speed of 15 m/s and rotational speeds of 324.5 RPM and 424.5 RPM, corresponding to tip speed ratios of 5.1 and 6.7, respectively. The details of the MEXICO turbine can be found in Refs [27,28].

Blade oscillation is incorporated into the flow modelling. Modal analysis conducted prior to the flow simulation provides the blade's natural vibration frequency and structural mode shapes. In a forced response and flutter analysis of turbomachinery, the structural motion of the blade is typically dictated by the natural frequencies and the corresponding mode shapes of the blade structure. To be consistent with the authors' previous studies, the first natural frequency, obtained from the modal analysis, is employed as the vibration frequency. The first natural frequency corresponds to the fundamental vibration mode, which typically carry the highest energy and is most susceptible to resonance, posing a significant risk of structural failure. In particular, the first vibration mode, which includes primary blade motions, is highly influenced by operational and environmental conditions. These modes are crucial for assessing aeroelastic stability to ensure structural integrity. Consistent with previous work [26], the first natural frequency of 15.611 Hz and its corresponding mode shape are selected to represent the blade's vibration. A realistic vibration amplitude for a modern offshore wind turbine which is equivalent to 9% of the blade span is used in the flow simulation. Since the blades of offshore wind turbines are getting longer and more flexible, the structural deformation can be significantly large. Studies suggest that the deflection of the blade can be as large as 9% of the blade radius, which is a significant figure for modern offshore wind turbines [29]. Therefore, the amplitude of 9% span is selected for this study. The blades are considered to be vibrating out of phase with each other, and the phase angle between the blades is 120°. The tower structure is also included to model the interaction between the stationary structure and the rotating blade. A detailed description of the MEXICO wind turbine and the model used in this study is presented in Figure 1. The figure shows the physical model of the wind turbine with blades oscillating at an amplitude of 9% span and a frequency of 15.611 Hz.

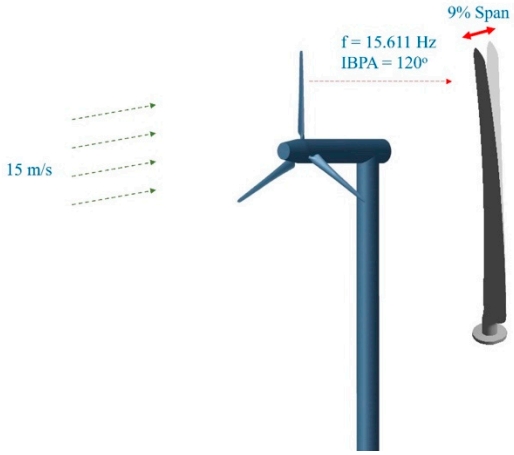

Figure 1. Illustration of the MEXICO wind turbine model and the blade used in the simulation (Presented in [30]).

3. Methodologies

An aeroelastic analysis involves aerodynamic modelling and structural modelling, and they are coupled together to model the interaction between the fluid flow and the structural responses. Table 1 summarises some of the widely used methods for the aeroelastic modelling of wind turbines. A novel nonlinear frequency-domain solution method has been explored for the aeroelastic modelling of wind turbines, integrating CFD for the aerodynamic modelling and FEA for the structural modelling to efficiently capture the interaction between the unsteady aerodynamic flow field and the turbine structures. This approach enables accurate prediction of aerodynamic loads and turbine response to varying wind conditions while significantly reducing computational costs compared to traditional time-domain simulations. Another distinctive feature of this study is to evaluate the aerodynamic and aeroelastic performances of a complete wind turbine model with the blades experiencing a flutter behaviour under different operating conditions using a nonlinear frequency-domain solution method. CFD simulations are conducted using Cadence Fine Turbo 2024.1 and FEA simulations are performed using ANSYS Mechanical 2024R2.

Table 1. Numerical methods used for the aeroelastic modelling of wind turbines.

Numerical Methods	Refs
Aerodynamic modelling	
1. Blade Element Momentum (BEM) model	[31,32]
2. Vortex model	[12,33]
3. Actuator-type model	[16,34]
4. Computational Fluid Dynamics (CFD) model	[21,35]
Structural modelling	
1. Beam model	[36,37]
2. Multi-body dynamics (MBD) model	[38,39]
3. Computational Structural Dynamics (CSD) model	[23,24]
4. Finite Element Analysis (FEA) model	[40,41]

3.1. Flow Governing Equations

Flow modelling is carried out using a three-dimensional, density-based, finite-volume flow solver. The Navier–Stokes equations governing the flow can be expressed in a Cartesian domain as follows:

$$\frac{\partial}{\partial t}\int_V Q dV + \int_A \vec{F}_I \,.\, d\vec{A} + \int_A \vec{F}_V \,.\, d\vec{A} = \int_V S dV \quad (1)$$

where V is the volume, A is the surface, S is the source term, Q is the vector of the flow variables, and $\vec{F}_I$ and $\vec{F}_V$ are the inviscid and viscous flux vectors, respectively. The equation can be simplified as follows:

$$\frac{\partial}{\partial t}(Q) = R(Q) \tag{2}$$

In this equation, R represents combined residual and source terms. The Spalart–Allmaras or SA model, proposed in [42], is used for the turbulence modelling. The Spalart–Allmaras turbulence model is selected due to its established suitability for external aerodynamic flows using a structured gird, especially those dominated by wall-bounded shear layers, a characteristic of the present wind turbine simulations. This choice is further supported by prior experience with similar wind turbine analyses [26], where the model has yielded good agreement with experimental data and reliably predicted aerodynamic loads and aeroelastic behaviour.

In this study, the modelling of the flow and aeroelasticity analysis of wind turbines is carried out using a nonlinear frequency-domain method. By using the frequency-domain solution approach, the Fourier series can be applied to represent the conservative flow variables Q based on a specified fundamental frequency ω and a prescribed number of harmonics n as described below:

$$Q = \overline{Q} + \sum_{harmonic=1}^{n} \left[\alpha_Q \sin(n\omega t) + \beta_Q \cos(n\omega t)\right] \tag{3}$$

In this equation, $\overline{Q}$ is the time-averaged or mean parameter, and the Fourier coefficients of the conservations are represented by α_Q and β_Q. The applied numerical methods use the order of the Fourier series or number of harmonics in this case, as an input parameter and the accuracy of the unsteady solution can be achieved by controlling the order of the Fourier series. To model the unsteady flow in the frequency domain, the above Fourier decomposition is substituted into the original Navier–Stokes equation (i.e., Equation (2)) to generate the new set of unsteady Navier–Stokes equation in the frequency domain as follows:

$$\omega \sum_{harmonic=1}^{n} \left[n\alpha_Q \cos(n\omega t) - n\beta_Q \sin(n\omega t)\right] = R \tag{4}$$

The new sets of Navier–Stokes equations (Equation (4)) are solved simultaneously in the frequency domain using the frequency-domain solution method. The unsteady period is divided evenly into $N = (2n + 1)$ time intervals and an iterative method is used to solve the system of nonlinear equations coupling all N levels. The fundamental mode (one harmonic) is used in this paper as the source of flow unsteadiness mainly due to the periodic blade displacement. By using one harmonic, the above Equation (3) becomes the following:

$$Q = \overline{Q} + \left[\alpha_Q \sin(\omega t) + \beta_Q \cos(\omega t)\right] \tag{5}$$

The detailed formulation of the nonlinear frequency-domain solution can be found in [25,26].

3.2. Fluid–Structure Interaction

The modal coupling method is then applied to integrate the vibration of the blade into the flow modelling to carry out the aeroelastic analysis of the wind turbine. The equation governing the solid mechanics of the blade structure can be expressed as follows:

$$\boldsymbol{m\ddot{u}} + \boldsymbol{c\dot{u}} + \boldsymbol{ku} = \boldsymbol{f} \tag{6}$$

where $\boldsymbol{m}$ is the mass matrix, $\boldsymbol{c}$ is the damping matrix, $\boldsymbol{k}$ is the stiffness matrix, $\boldsymbol{u}$ is the displacement, and $\boldsymbol{f}$ is the external load acting on the structure.

The global displacement of the structure can be expressed by the following:

$$\mathbf{u} = \sum_{i=1}^{n_{modes}} d_i \, \boldsymbol{\theta_i} \tag{7}$$

where d_i is the generalised displacement of the structure and $\boldsymbol{\theta_i}$ is the mass normalised mode shapes.

By incorporating Equation (7) into the modal equation, assuming Rayleigh damping, and choosing a suitable scale factor for the mode shape, a set of independent equations for each mode can be expressed as follows:

$$\ddot{d}_i + 2\xi_i\omega_i\dot{d}_i + {\omega_i}^2 d_i = \boldsymbol{\theta_i}^T \boldsymbol{f} \tag{8}$$

In this equation, ω_i and ξ_i are the natural frequencies and the damping coefficients for each mode, respectively.

Before the flow simulation is carried out, the modal analysis is conducted using an FEA method to calculate the natural frequencies and structural mode shapes. The results of the modal analysis are then transferred to the flow simulation to compute the vibration of the blades. d_i can be written as follows:

$$d_i(t) = \overline{d} + d_A \cos(\omega_i t) \tag{9}$$

where $\overline{d}$ is the mean value, and d_A is the amplitude of the generalised displacement.

3.3. Computational Domain and Grid

Figure 2 shows the three-dimensional domain and grid structure developed for this study. The rotor and the tower are modelled in separate domains that are meshed individually. The computation domain of the complete wind turbine is created by connecting these two domains using a rotor-stator interface. A structured multi-block grid, suitable for the present computations, is generated with Cadence AutoGrid using an O4H topology. This topology refers to a specific type of structured multi-block grid, and it typically combines the advantages of two simple grid topologies such as an O-grid which wraps around an aerofoil or a blade with a circular or elliptical shape grid and an H-grid which is a more rectangular or block-like grid and often used for the regions away from the blade. The employed gird in this study comprises five blocks: an O-mesh skin block surrounding the blade; H-mesh inlet and outlet blocks positioned upstream of the leading edge and downstream of the trailing edge, respectively; and H-mesh upper and lower blocks located above and below the blade section, as shown in Figure 2. The thickness for the first cell layer at the boundaries of the rotor and the tower is set at 1×10^{-5} m ensuring that y^+ value is less than one to accurately compute the flow at the boundary layer.

In the traditional time-domain solution method, the flow needs to be modelled at all three blades using a 360° domain, while the frequency-domain solution method requires only one rotor blade (120° domain) and the flow harmonics for the remaining blades can be phase-shifted between periodic boundaries. The inlet of the domain is set at 4R (where R is the rotor radius) upstream of the rotor and the outlet at 8R downstream of the rotor. The far-field or external boundaries are located at a distance of 3R from the centre of the rotor. 4.5×10^6 elements are used to generate a 120° domain for each rotor passage and 14×10^6 elements are used to generate the tower domain. Therefore, the combined number

of elements for the time-domain method and the frequency-domain method are 27.5 million and 18.5 million, respectively.

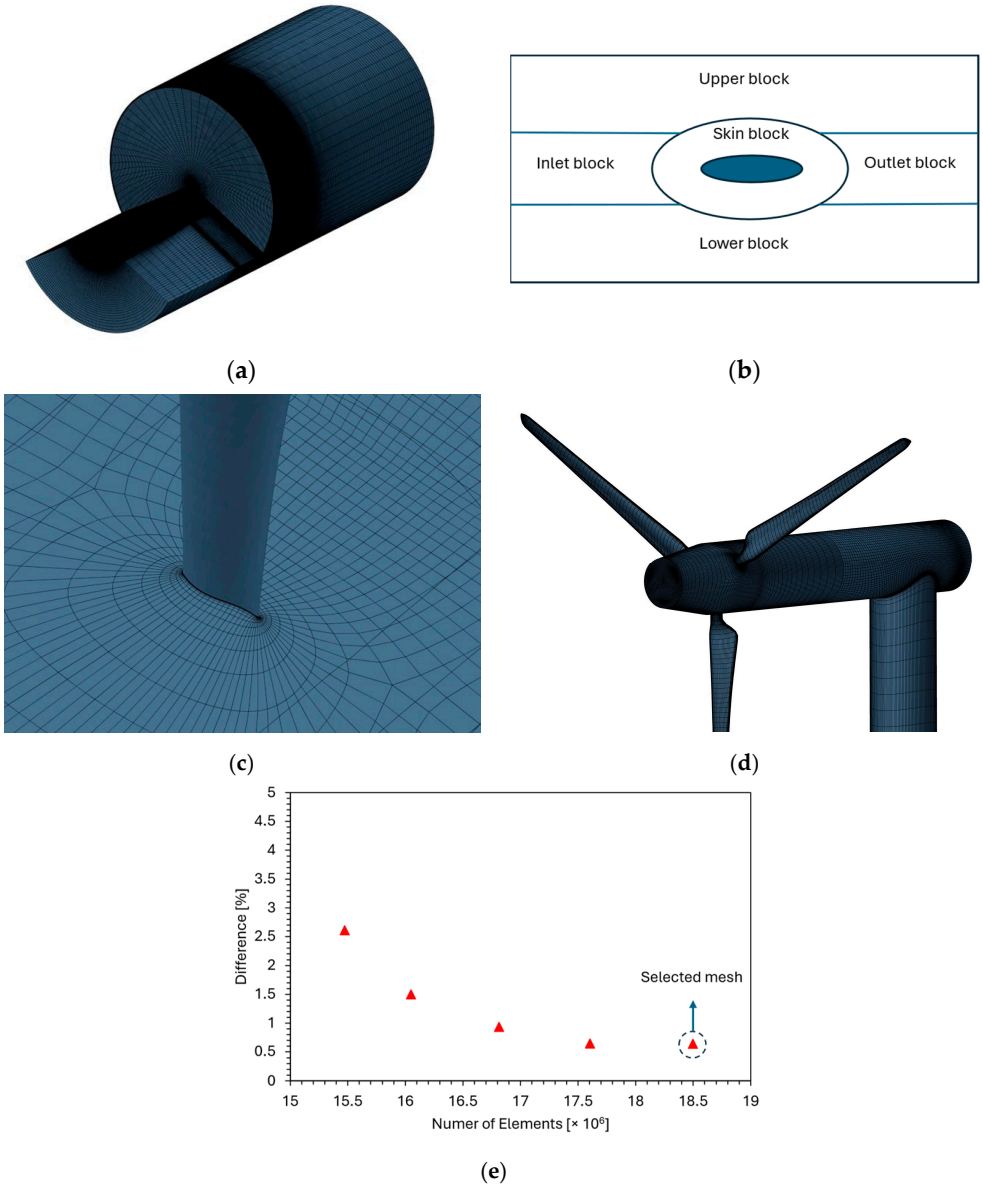

Figure 2. Mesh structure for computational domain showing: (**a**) overall mesh, (**b**) schematic diagram of an O4H topology, (**c**) blade-to-blade mesh, (**d**) solid mesh in 3D, and (**e**) mesh sensitivity study.

Figure 2e illustrates the effect of the combined rotor with a single blade and tower grid resolution on the blade load calculations, specifically torque. The results show that increasing the grid size beyond 17 million points yields less than a one percent improvement. Therefore, the final grid resolution of 18.5 million, which corresponds to 27.5 million with all three blades, employed in this study is considered adequate for the present analysis.

3.4. Boundary Conditions and Numerical Scheme

The surfaces of the rotor blade, the tower, and the hub are set as solid wall boundaries with a no-slip condition. The deforming wall boundary condition having a periodic displacement is applied on the blade in this analysis to facilitate an aeroelastic analysis.

A far-field boundary condition is applied to the external boundaries of the computational domain to simulate the external flow. While all three blades are modelled in the time-domain approach, it is unnecessary with the frequency-domain method where a

periodic boundary condition is employed. The rotor and tower domains are connected using a non-matching rotor-stator interface to create the complete wind turbine model. The interface is implemented using a nonlinear harmonic method in the frequency-domain approach and a sliding-plane method in the time-domain approach. The time-domain method requires a full three-bladed rotor model to simulate the blades vibrating at a phase angle of 120°. The frequency-domain method, however, calculates the mean unsteady flow and harmonic components for a single blade and then phase-shifts these values across periodic boundaries using an Inter Blade Phase Angle (IBPA), as described in [25].

The spatial discretisation and the temporal discretisation of the flow governing equations are carried out using a second-order accurate central scheme and a four-step Runge–Kutta scheme, respectively.

3.5. Validation

The validation of the CFD model was rigorously performed by comparing the predicted pressure coefficient (C_p) distributions with the experimental measurements and the data from an established reference simulation [43], as shown in Figure 3. The MEXICO rotor is a well-documented and widely studied benchmark case in wind energy research, providing a robust dataset for comparison. Bechmann et al. [43] presented detailed aerodynamic load predictions against experimental data, including pressure coefficients, which are directly relevant to the focus of our current work on aerodynamic load calculations. Their study offers a comprehensive set of data across a range of operating conditions, enabling a thorough assessment of the accuracy and reliability of our numerical approach. The comparison of C_p was conducted at multiple blade span sections, specifically at 25%, 35%, 60%, 82%, and 92% of the span to provide a comprehensive assessment of the performance of the model across the entire blade geometry. Examining C_p distributions at these diverse spanwise locations allows for a detailed evaluation of the ability of the model to capture variations in flow behaviour along the blade. While an excellent agreement between the CFD-predicted C_p values, the reference simulations, and the experimental data were observed at the 35%, 60%, 82%, and 92% span sections, slight variations were noted at the 25% section between the experiment and the simulations. These minor discrepancies are attributed to potential uncertainties associated with the pressure transducers used in the experimental setup at these specific locations, as discussed in [27,43]. Despite these localised variations, the strong correlation observed at the majority of spanwise locations indicates that the CFD model accurately captures the dominant pressure field and associated flow physics over the blade surface, including key features such as pressure gradients and stagnation points. The consistent agreement across the majority of sections validates the overall accuracy of the model and enhances confidence in its predictive capabilities for further analysis involving blade structural vibration at different operating conditions.

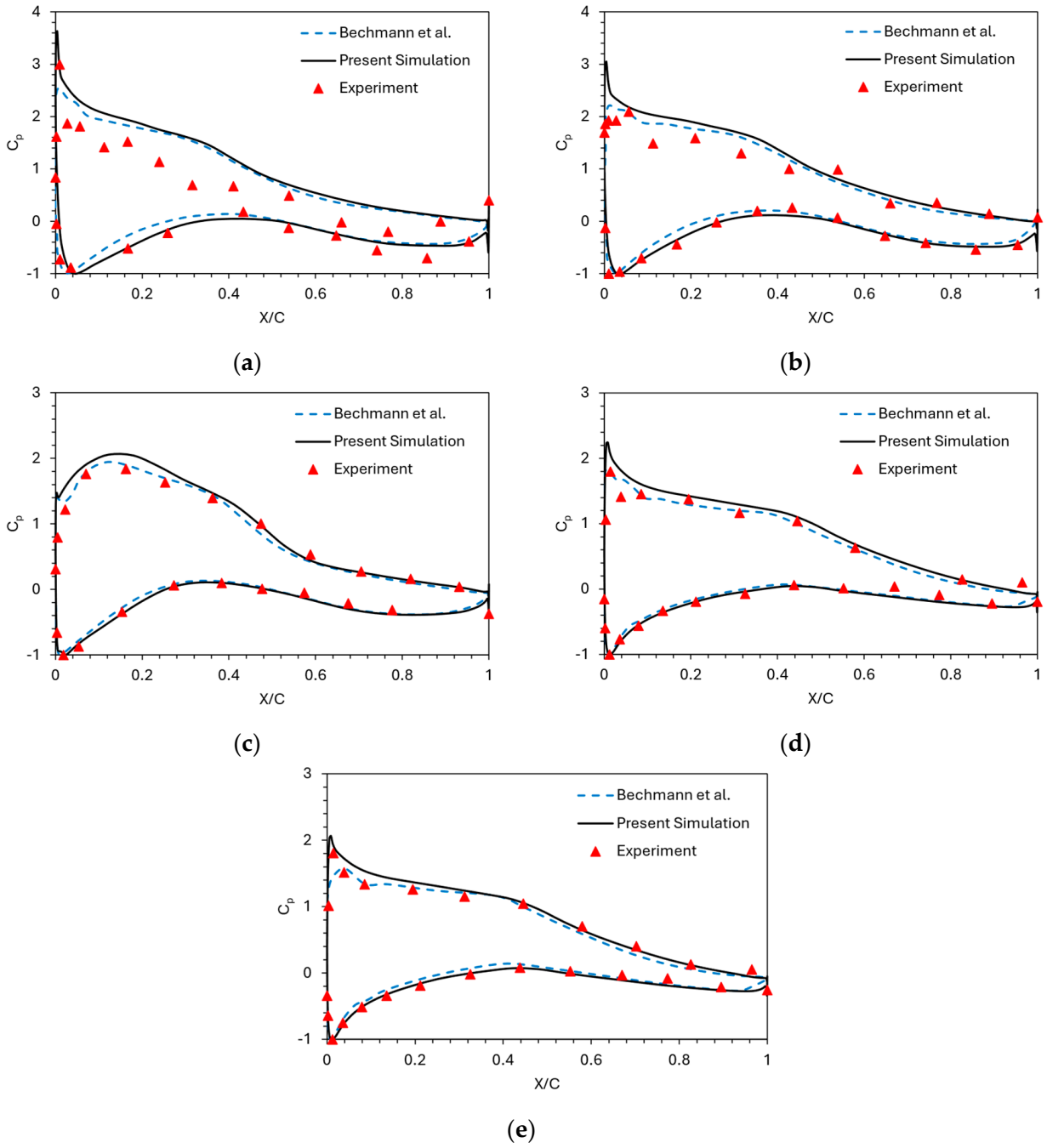

Figure 3. Distribution of steady pressure coefficient (C_p) over the blade surfaces at (**a**) 25% span, (**b**) 35% span, (**c**) 60% span, (**d**) 82% span, and (**e**) 92% span sections, obtained by the experiment, the reference simulation of Bechmann et al. [43], and the present simulation.

4. Results and Discussion

4.1. Aeroelastic Analysis of the MEXICO Wind Turbine

After an agreement between the CFD model and the experiment is achieved, the numerical simulations of a complete wind turbine with blades experiencing a relatively large amplitude of oscillation are carried out. The vibration frequency of 15.611 Hz is integrated into the simulations. This study discusses both aerodynamic and aeroelastic characteristics of wind turbines subjected to the effect of the interaction between the unsteady flow and the oscillation of turbine blades. The aeroelastic analysis of the complete wind turbine is conducted using the nonlinear frequency-domain solution method. The

results of the proposed frequency-domain method are also validated by conducting a similar complete simulation in the traditional time domain. The resulting displacement contours of the turbine blades are shown in Figure 4. The figure, which is obtained from the frequency-domain solution, shows that only a single blade needs to be modelled in the frequency-domain solution method as the displacements are phase-shifted between periodic boundaries by an IBPA of 120°.

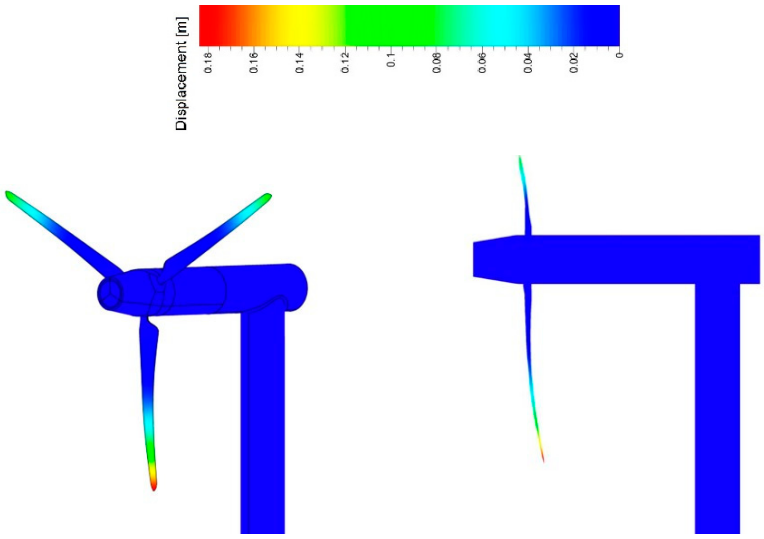

(**a**) (**b**)

Figure 4. Contour showing the displacement of wind turbine blades in (**a**) isometric view, and (**b**) side view (presented in [30]).

4.1.1. Unsteady Pressure Distribution

Blade vibration is a significant factor contributing to the formation of unsteady pressure fluctuations on the blade surface. Understanding these unsteady pressure dynamics is crucial for predicting blade fatigue, noise generation, and overall aerodynamic performance. This behaviour is analysed by examining the unsteady pressure amplitude coefficient, which quantifies the magnitude of these pressure fluctuations. Figure 5 presents the unsteady pressure amplitude coefficient at 25%, 60%, and 92% span sections for rotational speeds of 424.5 RPM and 324.5 RPM. These specific span sections were chosen to represent the flow behaviour near the blade root (25%), mid-span (60%, and tip (92%), providing a comprehensive understanding of the unsteady pressure distribution along the blade.

The aeroelastic simulations of the MEXICO wind turbine are mainly conducted using the frequency-domain solution method. The accuracy of the method is validated against the time-domain solution method as the experimental data are not available. Since the blade undergoes vibration, the fluctuations of the unsteady pressure are observed over the blade surfaces. The unsteady pressure can be expressed based on the Fourier series as below.

$$P = \overline{P} + P_A \sin(\omega t) + P_B \cos(\omega t) \tag{10}$$

In this equation, $\overline{P}$ is the time-averaged pressure, and P_A and P_B are the Fourier coefficients. The unsteady pressure amplitude (P_{Amp}) can be calculated from the Fourier coefficients. P_{Amp} is expressed as follows:

$$P_{Amp} = \sqrt{{P_A}^2 + {P_B}^2} \tag{11}$$

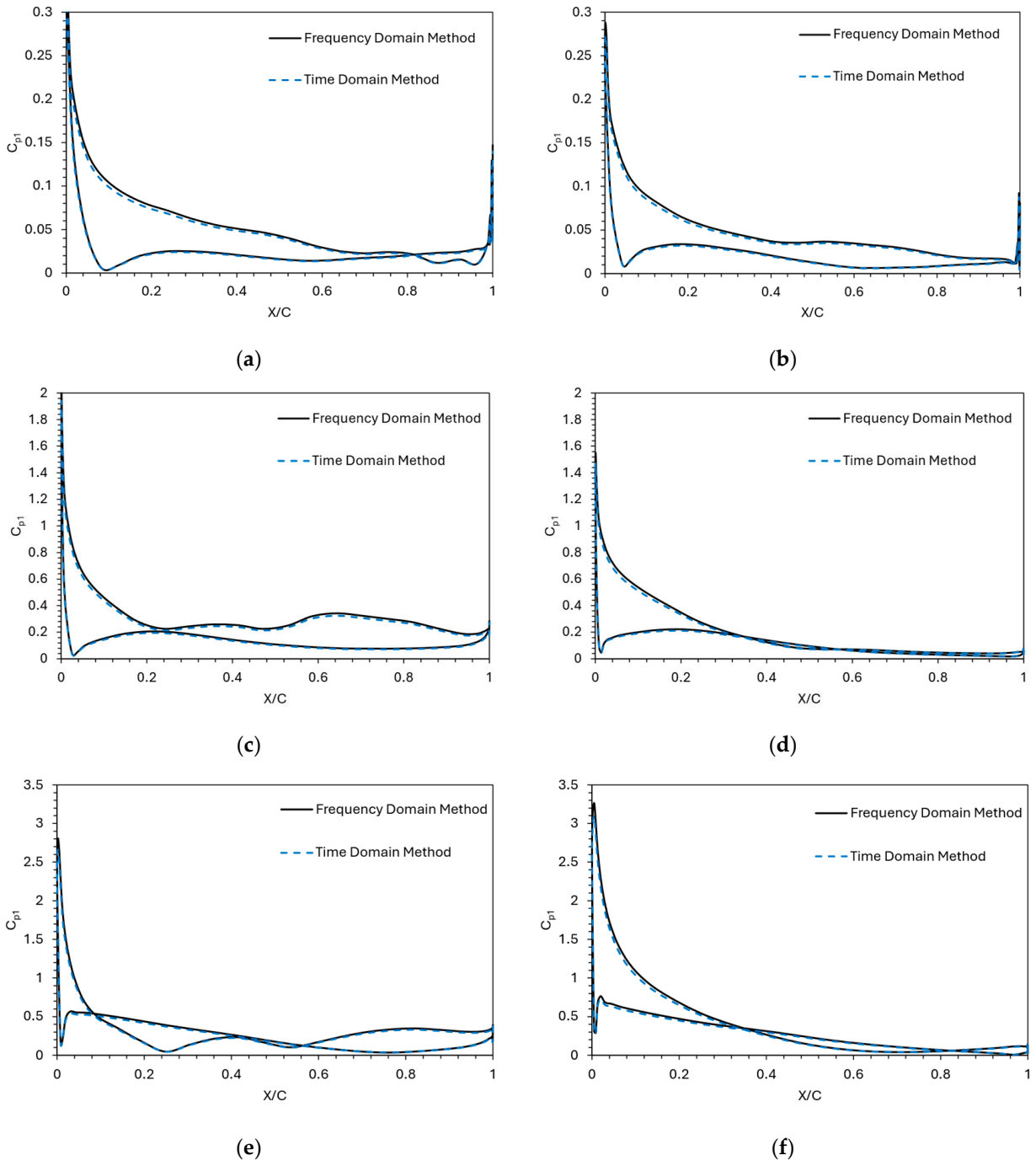

Figure 5. Distribution of unsteady pressure amplitude coefficient (C_{pl}) at (**a**) 25% span at 324.5 RPM, (**b**) 25% span at 424.5 RPM, (**c**) 60% span at 324.5 RPM, (**d**) 60% span at 424.5 RPM, (**e**) 92% span at 324.5 RPM, and (**f**) 92% span at 424.5 RPM.

The unsteady pressure amplitude coefficient, C_{p1}, can be calculated by dividing the amplitude by the dynamic pressure. Figure 5a,b present the unsteady pressure amplitude coefficient, computed by both the frequency-domain and time-domain solution methods, at the rotational speeds of 324.5 RPM and 424.5 RPM, respectively. The analysis of the blade reveals unsteady pressure fluctuations at both 324.5 RPM and 424.5 RPM due to the blade structural oscillation. While unsteady pressure implications are strongly present at 324.5 RPM, the distribution at 424.5 RPM is more consistent across the blade span, except 25% span at the blade root region where the local angle of attack of the aerofoil is large. Notably, the unsteady pressure magnitude is stronger in the blade tip region

where the oscillation amplitude of the blade is higher with a displacement of 9% span. This concentration of unsteady pressure at the tip suggests susceptibility to the unsteady flow phenomena, potentially related to tip vortex shedding and aeroelastic effects. Despite the fact that the unsteady pressure amplitude is higher at 424.5 RPM due to its higher tip speed, the distribution of pressure is more complex and inconsistent over the blade surfaces at 324.5 RPM which causes implications for the unsteady aerodynamic load which directly contributes to the aerodynamic damping which will be discussed next in this paper.

A key aspect of this study is the comparison of results obtained using the proposed frequency-domain method with those from the traditional time-domain method. Time-domain methods, while accurate, can be computationally expensive, particularly for complex geometries and transient simulations. Frequency-domain methods offer a more efficient alternative by analysing the unsteady pressure response in the frequency domain. The close agreement observed between the two approaches, as shown in Figure 5, validates the accuracy and applicability of the frequency-domain method for capturing the unsteady pressure distribution on the blade surfaces caused by blade vibration. This is particularly advantageous for parametric studies and design optimisation processes as it provides an efficient and reliable alternative to time-consuming time-domain methods.

The contours of instantaneous pressure on the pressure and suction surfaces of the turbine blades are shown in Figure 6. It can be seen that all three turbine rotor blades possess similar pressure distributions on the blade surface. However, one of the blades is observed to have a relatively higher pressure difference compared to the other two blades. This phenomenon is detected due to the blade vibration at an inter-blade phase angle causing different pressure distributions on the surfaces of each blade. In the frequency solution domain, this behaviour is captured by modelling only one blade and phase-shifting the flow quantities between periodic boundaries by 120°.

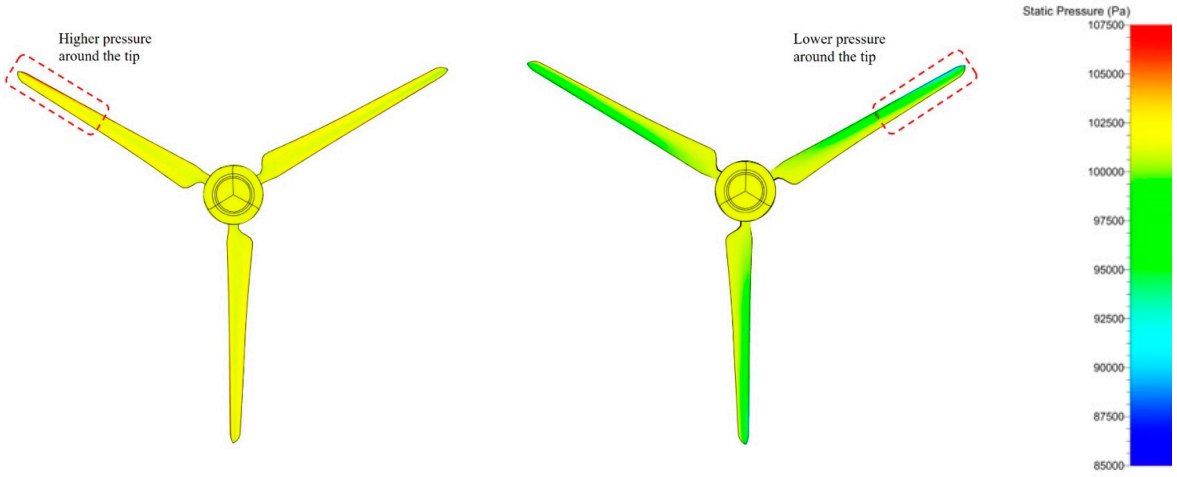

(**a**) (**b**)

Figure 6. Contour showing pressure distribution over the blade at (**a**) pressure surface, and (**b**) suction surface (presented in [30]).

Figure 7 demonstrates the unsteady pressure amplitude contours exported from the frequency-domain solutions at the rotational speeds of 324.5 RPM and 424.5 RPM, respectively. These contours provide a visual representation of the spatial distribution of unsteady pressure fluctuations across the blade surface to provide insights into the dynamic loading experienced by the blade. At the lower rotational speed of 324.5 RPM, the unsteady pressure amplitudes are relatively low compared to that of 424.5 RPM. However, an increase in unsteady pressure amplitude is observed at the higher rotational speed of 424.5 RPM. As expected, the highest amplitudes are concentrated within the blade tip

region where the blade oscillation amplitude is higher with the tip displacement of 9% span. This concentration of unsteady pressure at the tip strongly indicates that this region is particularly vulnerable to unsteady flow phenomena, such as tip vortex shedding and strong vortex generation, which are exacerbated at higher rotational speeds. Although the amplitude of the unsteady pressure is higher at 424.5 RPM, it was seen in Figure 5 that the distribution of the unsteady pressure is more complex and inconsistent at 324.5 RPM than at 424.5 RPM. The observed complication in unsteady pressure amplitude has important implications for both structural integrity and aerodynamic performance of the blade.

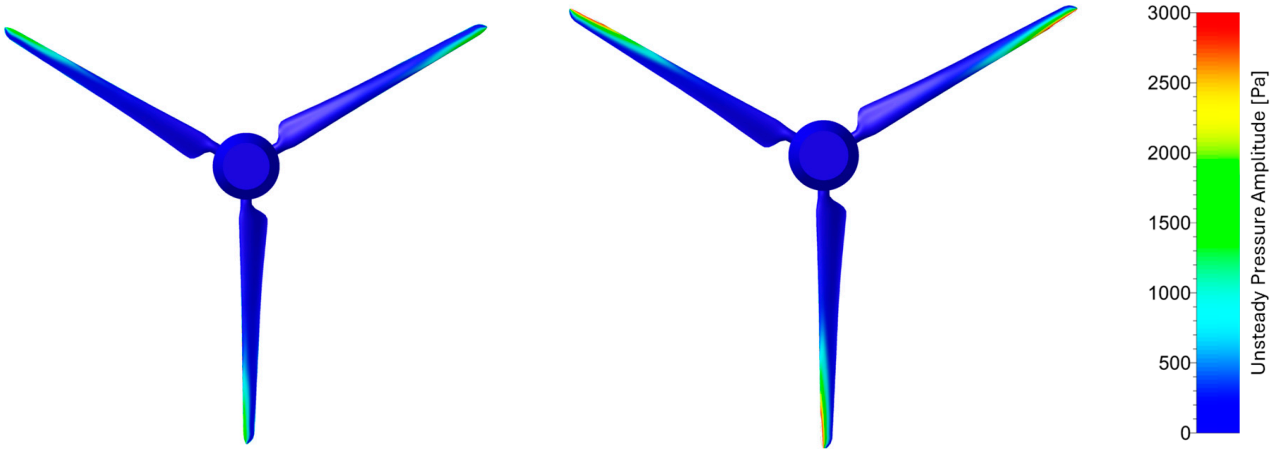

(**a**) (**b**)

Figure 7. Unsteady pressure amplitude contours at (**a**) 324.5 RPM, and (**b**) 424.5 RPM.

4.1.2. Aerodynamic Damping

The aerodynamic power of a wind turbine blade is a crucial factor in the analysis of aeroelastic stability. Figure 8 indicates that the wind turbine blade exhibits a dominant stability effect at 424.5 RPM, particularly notable at the tip region where the oscillatory amplitudes are the largest. This stability is intrinsically linked to the aerodynamic power generated by the blade. The negative aerodynamic power in the figure suggests that the aerodynamic forces acting on the blade effectively dampen vibrations, especially at the tip, where the linear velocity is highest and even small changes in the angle of attack can impact the aerodynamic damping forces. At 324.5 RPM, a similar distribution in the aerodynamic power is observed; however, the magnitudes are relatively less than that of 424.5 RPM.

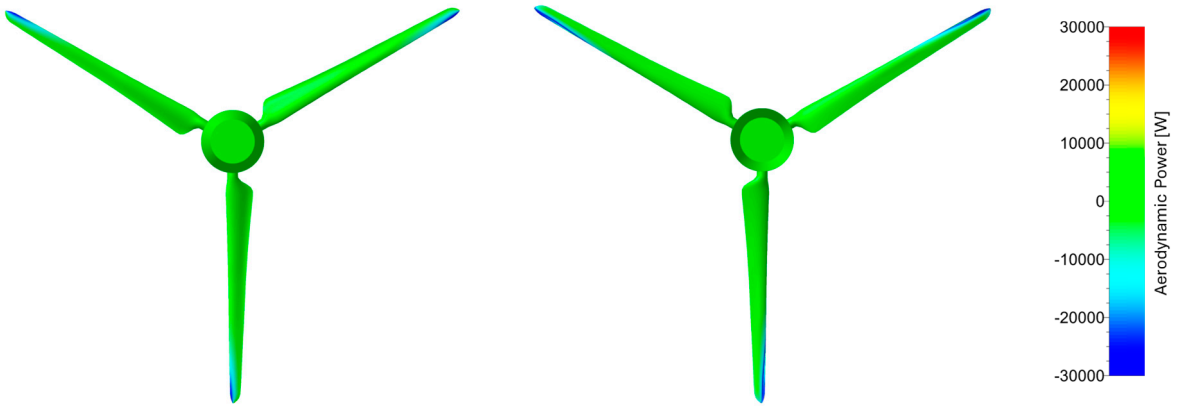

(**a**) (**b**)

Figure 8. Aerodynamic power contours at 424.5 RPM at (**a**) pressure surface, and (**b**) suction surface.

However, it is crucial to recognise that the overall aerodynamic damping is a critical parameter to identify sources of instability under certain conditions. For instance, rapid changes in wind speed or direction can induce fluctuations in aerodynamic loading, potentially leading to resonant vibrations and aeroelastic instability. Therefore, a key emphasis of the present study is to determine the aerodynamic damping, quantified as the work performed per vibration cycle, to assess the aeroelastic response of the blade to varying operational conditions, and to detect potential instabilities. This is typically achieved by establishing a transient periodic solution. This approach allows for the assessment of system stability across various blade vibration frequencies. The work per vibration cycle, representing the energy exchanged between the blade and the surrounding airflow during one oscillation, can be calculated as follows:

$$W = \int_{t_0}^{t_0+T} \int_A p\vec{v}.\hat{n}dAdt \tag{12}$$

where W is the aerodynamic work per cycle, T is the period of one oscillation cycle, p is the fluid pressure, $\vec{v}$ is the velocity due to imposed oscillational displacements, $\hat{n}$ is the unit vector, and A is the surface area. The aerodynamic damping can then be calculated by normalising the aerodynamic work per cycle by $m_m\omega_v^2 D_{max}^2$ where m_m is the modal mass, ω_v is the vibration frequency, and D_{max} is the maximum displacement amplitude as discussed in [26]. Table 2 shows the aerodynamic damping computed from the time-domain and frequency-domain methods for two rotational speeds while the blade is oscillating at an amplitude of 9% span. The results demonstrate positive aerodynamic damping values for both rotational speeds considered (324.5 RPM and 424.5 RPM), which indicate aeroelastic stability within these operational regimes. However, a notable difference in damping magnitude is observed between the two rotational speeds. The aerodynamic damping at 324.5 RPM is considerably lower than that for 424.5 RPM, which suggests a strong correlation between the unsteady pressure distribution seen in Figure 5 and the aerodynamic damping. A complex and inconsistent distribution of unsteady pressure amplitude was observed for the case of 324.5 RPM compared to the 424.5 RPM case. This difference in unsteady pressure distribution directly correlates with the observed variation in aerodynamic damping. The more complex and inconsistent pressure distribution at 324.5 RPM likely results in less effective energy dissipation from the vibrating blade, leading to lower aerodynamic damping values compared to the pressure field at 424.5 RPM. Furthermore, the close agreement between aerodynamic damping values computed using both time-domain and frequency-domain methods provides strong validation for the accuracy and reliability of the frequency-domain approach employed in this study.

Table 2. Aerodynamic damping obtained by the frequency-domain method and the time-domain method.

Case	Frequency-Domain Method	Time-Domain Method
At 324.5 RPM	0.237	0.225
At 424.5 RPM	0.108	0.103

4.1.3. Flow Visualisation

The relative velocity vector around the wind turbine rotor blade, with the contours of instantaneous pressure distribution is plotted in Figure 9. The figure clearly shows the relation between the velocity vector and the static pressure distribution around the turbine blade surface. When the incoming flow with the relative wind velocity encounters the aerofoil of the turbine blade, it causes the airflow to be diverted from the leading edge of the aerofoil and the flow is distributed across the blade pressure and suction surface. As seen

in Figure 9, the suction surface of the blade has a higher velocity distribution. However, the high-pressure distribution is observed on the pressure surface of the blade, particularly near the leading and trailing edge of the turbine blade. This behaviour indicates the blade generating a lift force as it rotates. Moreover, the presence of blade vibration further intensifies the velocity vector distortion, leading to a noticeable fluctuation of pressure and velocity around the surface of the aerofoil.

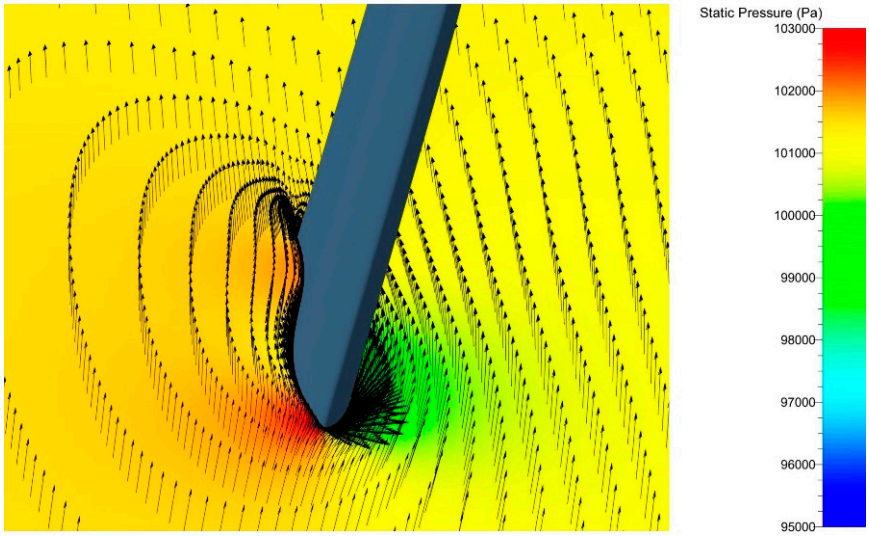

Figure 9. Velocity vector distribution in the surroundings of the rotor blade (presented in [30]).

The aerodynamic characteristics of the flow around the wind turbine are affected noticeably by the presence of the turbine structure. This impact can be seen clearly in the velocity distribution around the turbine blades and the formation of wake patterns as shown in Figure 10. In this figure, the distortion of the flow due to the presence of blade vibration is clearly seen. Moreover, the presence of the tower causes the distortion of the flow forming the vortex patterns along the length of the tower. The rotor hub also caused the formation of vortex structures as observed in Figure 10. The hub vortices formed are then combined with the rotor vortices as the flow passes through. The wake region downstream of the rotor is affected by the presence of vibration in the blade structure which introduces turbulence and energy to the flow surrounding the turbine blade.

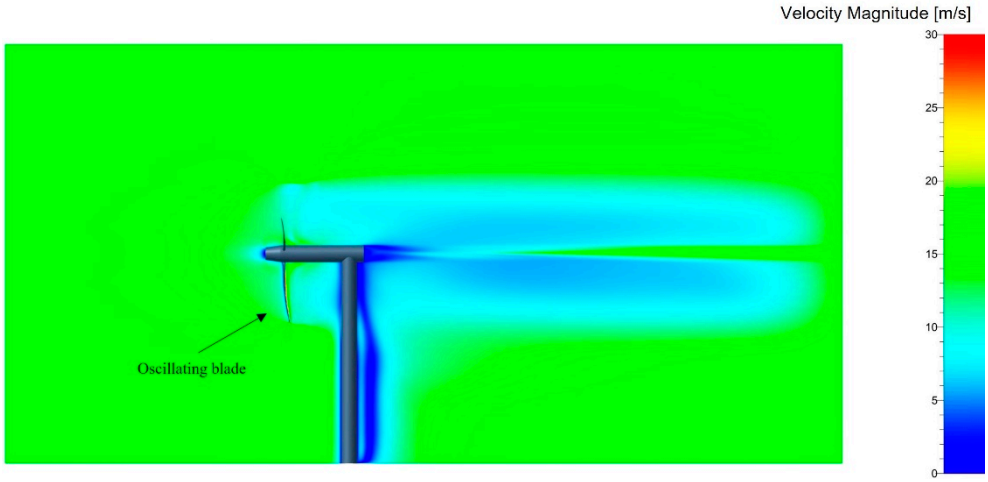

Figure 10. Development of the velocity field and downstream wake of the wind turbine (presented in [30]).

The interaction between the rotating and stationary components of the turbine causes the formation of unsteady flow around the turbine. The formation of tip vorticity around the rotor blade and the flow streamlines surrounding the turbine can be observed in Figure 11. The rotation of the rotor blades generates the vortices at the tip of the rotor and can be observed in Figure 11a. The vorticity diffusion and advection are clearly observed in this figure. As those tip vortices interact with the stationary tower, the vortex structures deform, leading to the formation of additional wake structures and an increase in flow turbulence as they progress downstream of the flow. As seen in Figure 11b, the tower structure affects the velocity streamlines passing through the blades and causes part of the velocity streamlines to attach to the structure forming the tower vortices downstream of the tower. Furthermore, the additional disturbances in the flow are caused by the interaction between the rotating turbine blades and the tower, leading to the formation of unstable and disorganised flow streamlines in the wake region of the turbine.

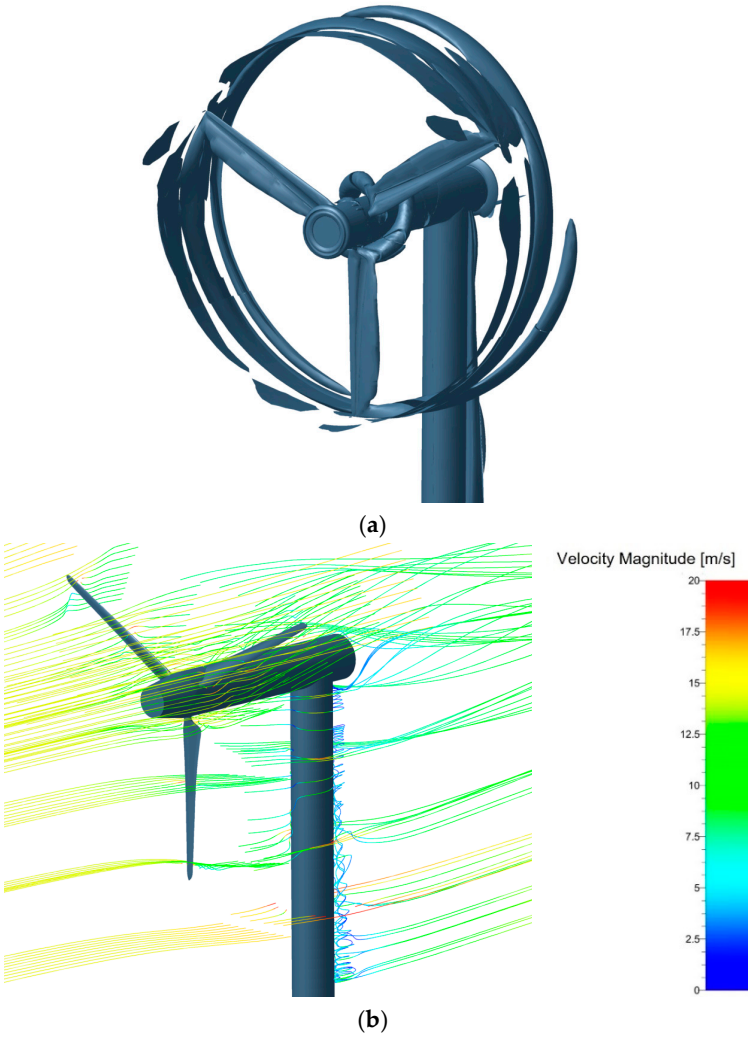

Figure 11. (**a**) Tip vorticity and (**b**) flow streamline development around the wind turbine (presented in [30]).

This study is primarily carried out using the nonlinear frequency-domain solution method and all the flow visualisation figures are exported from the frequency-domain solution. The figures from the time-domain solutions are not included to keep the paper concise as they are similar. The results proved that the frequency-domain solution method can be used reliably to model and capture the characteristics of unsteady flow associated with the interaction between the turbine blades and the unsteady flow. In the

traditional time-domain solution method, all three blades need to be modelled to capture this flow behaviour, which requires more computational power and is time-consuming. The frequency-domain solution method has a great advantage over the time-domain solution method as it is more computationally efficient without compromising the accuracy of the results.

4.2. Computational Costs

A computer powered by an Intel (R) Xeon (R) w9-3475X, 2208 MHz CPU with 36 cores and 72 logical processors is used for modelling and simulation of the wind turbine under consideration in this study. With the nonlinear frequency-domain solution method, the simulation only takes around 9 h, compared to more than 120 h of simulations using the time-domain solution method. By using the frequency-domain solution method, the computation cost is lowered by one or two orders of magnitude, while maintaining the required level of accuracy. Therefore, the frequency-domain solution method proved to be a reliable and efficient substitute for conventional time-domain methods for the aerodynamic and aeroelastic modelling of wind turbines.

5. Conclusions

This paper investigates the aerodynamic and aeroelastic behaviour of a full wind turbine model experiencing significant blade vibration at a realistic oscillation amplitude of 9% span demanding a thorough analysis of coupled fluid–structure interactions. A key objective is to demonstrate the effectiveness of the proposed nonlinear frequency-domain solution method for an aeroelastic analysis, as a computationally efficient alternative to resource-intensive time-domain approaches.

A rigorous validation process ensured the reliability of the employed methodologies. First, the underlying CFD model, crucial for capturing the complex flow physics, was validated against both experimental measurements and a well-established reference simulation. Subsequently, the accuracy of the proposed frequency-domain aeroelastic method was assessed by comparing its predictions with results from a conventional time-domain method. The comparison focused on key aeroelastic parameters: aerodynamic damping as a crucial stability indicator, and unsteady pressure distributions on the blade surfaces, reflecting dynamic aerodynamic loads. The strong agreement between the frequency- and time-domain results validated the ability of the frequency-domain approach to accurately capture the unsteady pressure distribution and aerodynamic loads for the aeroelastic analysis of a wind turbine system.

A key finding concerned the influence of rotational speed on unsteady pressure and aerodynamic damping. At 324.5 RPM, a complex and inconsistent unsteady pressure distribution was more dominant compared to the pressure distribution at 424.5 RPM. This nature of unsteady pressure directly impacted aerodynamic damping and the stability of the wind turbine. While positive damping, indicating stability, was confirmed at both speeds, the magnitude at 324.5 RPM was significantly lower, which emphasises the crucial role of operational speed in determining the aeroelastic stability margins.

Analysis of the flow field revealed a clear relationship between relative velocity and static pressure distribution around the blade, with higher velocities on the suction side and higher pressures on the pressure side, particularly near the leading and trailing edges. Blade vibration further intensified velocity vector distortion, leading to noticeable pressure and velocity fluctuations. The flow interaction between the oscillating blades and the stationary tower led to complex unsteady flow patterns, including tower vortices and disorganised wake streamlines.

Finally, the study highlighted the computational advantages of the frequency-domain solution method, which only demands approximately 9 h of computation compared to 120 h for the time-domain simulation. This substantial reduction in computational cost makes the frequency-domain approach a highly attractive tool for routine aeroelastic analyses and parametric studies to enable more rapid design iterations and optimisations.

Author Contributions: Conceptualization, S.W.N. and M.R.; methodology, S.W.N. and M.R.; software, S.W.N.; validation, S.W.N.; formal analysis, S.W.N.; investigation, S.W.N.; writing—original draft preparation, H.S.; writing—review and editing, S.W.N. and M.R.; visualisation, S.W.N.; supervision, M.R.; funding acquisition, S.W.N. All authors have read and agreed to the published version of the manuscript.

Funding: This research was funded by The University of the West of England, grant number VCECR24-15.

Data Availability Statement: The data presented in this study are available on request from the corresponding author.

Acknowledgments: The authors would like to acknowledge the Vice Chancellor's Early Career Research (VCECR) Award awarded by the University of the West of England. The authors presented the preliminary results of this research at the 16th International Symposium on Unsteady Aerodynamics Aeroacoustics and Aeroelasticity of Turbomachines (ISUAAAT16).

Conflicts of Interest: Author Htet Shine was employed by the company Capula Ltd. The remaining authors declare that the research was conducted in the absence of any commercial or financial relationships that could be construed as a potential conflict of interest.

References

1. The UK Government. The Ten Point Plan for a Green Industrial Revolution. *Policy Report* **2020**. Available online: https://www.gov.uk/government/publications/the-ten-point-plan-for-a-green-industrial-revolution/title (accessed on 23 March 2022).
2. Labour Party. Labour Party Manifesto 2024. *Policy Report* **2024**. Available online: https://labour.org.uk/wp-content/uploads/2024/06/Labour-Party-manifesto-2024.pdf (accessed on 25 January 2025).
3. Adrijana Buljan. Mingyang Commissions 16 MW Offshore Wind Turbine with 260-Metre Rotor Diameter in China. *Online* **2023**. Available online: https://www.offshorewind.biz/2023/07/18/mingyang-commissions-16-mw-offshore-wind-turbine-with-260-metre-rotor-diameter-in-china/ (accessed on 25 January 2025).
4. Hansen, M.H. Aeroelastic Instability Problems for Wind Turbines. *Wind Energy* **2007**, *10*, 551–577. [CrossRef]
5. Micallef, D.; Rezaeiha, A. Floating Offshore Wind Turbine Aerodynamics: Trends and Future Challenges. *Renew. Sustain. Energy Rev.* **2021**, *152*, 111696. [CrossRef]
6. Özkan, R.; Genç, M.S. Aerodynamic Design and Optimization of a Small-Scale Wind Turbine Blade Using a Novel Artificial Bee Colony Algorithm Based on Blade Element Momentum (ABC-BEM) Theory. *Energy Convers. Manag.* **2023**, *283*, 116937. [CrossRef]
7. Yang, Y.; Bashir, M.; Michailides, C.; Li, C.; Wang, J. Development and Application of an Aero-Hydro-Servo-Elastic Coupling Framework for Analysis of Floating Offshore Wind Turbines. *Renew. Energy* **2020**, *161*, 606–625. [CrossRef]
8. Abdelkhalig, A.; Elgendi, M.; Selim, M.Y.E. Review on Validation Techniques of Blade Element Momentum Method Implemented in Wind Turbines. *IOP Conf. Ser. Earth Environ. Sci.* **2022**, *1074*, 012008. [CrossRef]
9. Buhl, M.L. *NREL New Empirical Relationship between Thrust Coefficient and Induction Factor for the Turbulent Windmill State*; NREL/TP-500-36834; National Renewable Energy Laboratory: Golden, CO, USA, 2005. [CrossRef]
10. Dowler, J.L.; Schmitz, S. A Solution-Based Stall Delay Model for Horizontal-Axis Wind Turbines. *Wind Energy* **2015**, *18*, 1793–1813. [CrossRef]
11. Otter, A.; Murphy, J.; Pakrashi, V.; Robertson, A.; Desmond, C. A Review of Modelling Techniques for Floating Offshore Wind Turbines. *Wind Energy* **2022**, *25*, 831–857. [CrossRef]
12. Lee, H.; Lee, D.-J. Numerical Investigation of the Aerodynamics and Wake Structures of Horizontal Axis Wind Turbines by Using Nonlinear Vortex Lattice Method. *Renew. Energy* **2019**, *132*, 1121–1133. [CrossRef]
13. Rodriguez, S.N.; Jaworski, J.W. Strongly-Coupled Aeroelastic Free-Vortex Wake Framework for Floating Offshore Wind Turbine Rotors. Part 1: Numerical Framework. *Renew. Energy* **2019**, *141*, 1127–1145. [CrossRef]
14. Rodriguez, S.N.; Jaworski, J.W. Strongly-Coupled Aeroelastic Free-Vortex Wake Framework for Floating Offshore Wind Turbine Rotors. Part 2: Application. *Renew. Energy* **2020**, *149*, 1018–1031. [CrossRef]

15. Breton, S.-P.; Coton, F.N.; Moe, G. A Study on Rotational Effects and Different Stall Delay Models Using a Prescribed Wake Vortex Scheme and NREL Phase VI Experiment Data. *Wind Energy* **2008**, *11*, 459–482. [CrossRef]
16. Arabgolarcheh, A.; Jannesarahmadi, S.; Benini, E. Modeling of near Wake Characteristics in Floating Offshore Wind Turbines Using an Actuator Line Method. *Renew. Energy* **2022**, *185*, 871–887. [CrossRef]
17. Sanvito, A.G.; Firpo, A.; Schito, P.; Dossena, V.; Zasso, A.; Persico, G. A Novel Vortex-Based Velocity Sampling Method for the Actuator-Line Modeling of Floating Offshore Wind Turbines in Windmill State. *Renew. Energy* **2024**, *231*, 120927. [CrossRef]
18. Sørensen, J.N.; Shen, W.Z.; Munduate, X. Analysis of Wake States by a Full-Field Actuator Disc Model. *Wind Energy* **1998**, *1*, 73–88. [CrossRef]
19. Troldborg, N.; Sørensen, J.N.; Mikkelsen, R. Actuator Line Simulation of Wake of Wind Turbine Operating in Turbulent Inflow. *J. Phys. Conf. Ser.* **2007**, *75*, 012063. [CrossRef]
20. Wang, L.; Liu, X.; Kolios, A. State of the Art in the Aeroelasticity of Wind Turbine Blades: Aeroelastic Modelling. *Renew. Sustain. Energy Rev.* **2016**, *64*, 195–210. [CrossRef]
21. Liu, Y.; Xiao, Q.; Incecik, A.; Peyrard, C.; Wan, D. Establishing a Fully Coupled CFD Analysis Tool for Floating Offshore Wind Turbines. *Renew. Energy* **2017**, *112*, 280–301. [CrossRef]
22. Wang, L.; Quant, R.; Kolios, A. Fluid Structure Interaction Modelling of Horizontal-Axis Wind Turbine Blades Based on CFD and FEA. *J. Wind Eng. Ind. Aerodyn.* **2016**, *158*, 11–25. [CrossRef]
23. Dose, B.; Rahimi, H.; Herráez, I.; Stoevesandt, B.; Peinke, J. Fluid-Structure Coupled Computations of the NREL 5 MW Wind Turbine by Means of CFD. *Renew. Energy* **2018**, *129*, 591–605. [CrossRef]
24. Dose, B.; Rahimi, H.; Stoevesandt, B.; Peinke, J. Fluid-Structure Coupled Investigations of the NREL 5 MW Wind Turbine for Two Downwind Configurations. *Renew. Energy* **2020**, *146*, 1113–1123. [CrossRef]
25. Rahmati, M.T.; He, L.; Li, Y.S. The Blade Profile Orientations Effects on the Aeromechanics of Multirow Turbomachines. *J. Eng. Gas Turbines Power* **2015**, *138*, 062606. [CrossRef]
26. Win Naung, S.; Rahmati, M.; Farokhi, H. Nonlinear Frequency Domain Solution Method for Aerodynamic and Aeromechanical Analysis of Wind Turbines. *Renew. Energy* **2021**, *167*, 66–81. [CrossRef]
27. Schepers, J.G.; Boorsma, K.; Munduate, X. Final Results from Mexnext-I: Analysis of Detailed Aerodynamic Measurements on a 4.5 m Diameter Rotor Placed in the Large German Dutch Wind Tunnel DNW. *J. Phys. Conf. Ser.* **2014**, *555*, 012089. [CrossRef]
28. Schepers, J.G.; Boorsma, K.; Cho, T.; Gomez-Iradi, S.; Schaffarczyk, A.; Jeromin, A.; Shen, W.Z.; Lutz, T.; Meister, K.; Stoevesandt, B.; et al. *Final Report of IEA Task 29, Mexnext (Phase 1): Analysis of MEXICO Wind Tunnel Measurements*; ECN-E-07-042; ECN: Petten, The Netherlands, 2014.
29. Horcas, S.G.; Debrabandere, F.; Tartinville, B.; Hirsch, C.; Coussement, G. Extension of the Non-Linear Harmonic Method for the Study of the Dynamic Aeroelasticity of Horizontal Axis Wind Turbines. *J. Fluids Struct.* **2017**, *73*, 100–124. [CrossRef]
30. Win Naung, S.; Rahmati, M. Numerical Investigation of Aeroelasticity of Wind Turbines Using a Nonlinear Frequency Domain Solution Method. In Proceedings of the 16th International Symposium on Unsteady Aerodynamics Aeroacoustics and Aeroelasticity of Turbomachines (ISUAAAT16), Toledo, Spain, 19–23 September 2022.
31. Wang, L.; Liu, X.; Renevier, N.; Stables, M.; Hall, G.M. Nonlinear Aeroelastic Modelling for Wind Turbine Blades Based on Blade Element Momentum Theory and Geometrically Exact Beam Theory. *Energy* **2014**, *76*, 487–501. [CrossRef]
32. Rafiee, R.; Tahani, M.; Moradi, M. Simulation of Aeroelastic Behavior in a Composite Wind Turbine Blade. *J. Wind Eng. Ind. Aerodyn.* **2016**, *151*, 60–69. [CrossRef]
33. Chattot, J.-J. Helicoidal Vortex Model for Wind Turbine Aeroelastic Simulation. *Comput. Struct.* **2007**, *85*, 1072–1079. [CrossRef]
34. Shen, W.Z.; Zhu, W.J.; Sørensen, J.N. Actuator Line/Navier–Stokes Computations for the MEXICO Rotor: Comparison with Detailed Measurements. *Wind Energy* **2012**, *15*, 811–825. [CrossRef]
35. Yu, D.O.; Kwon, O.J. Predicting Wind Turbine Blade Loads and Aeroelastic Response Using a Coupled CFD–CSD Method. *Renew. Energy* **2014**, *70*, 184–196. [CrossRef]
36. Arany, L.; Bhattacharya, S.; Adhikari, S.; Hogan, S.J.; Macdonald, J.H.G. An Analytical Model to Predict the Natural Frequency of Offshore Wind Turbines on Three-Spring Flexible Foundations Using Two Different Beam Models. *Soil Dyn. Earthq. Eng.* **2015**, *74*, 40–45. [CrossRef]
37. Faccio Júnior, C.J.; Cardozo, A.C.P.; Monteiro Júnior, V.; Gay Neto, A. Modeling Wind Turbine Blades by Geometrically-Exact Beam and Shell Elements: A Comparative Approach. *Eng. Struct.* **2019**, *180*, 357–378. [CrossRef]
38. Al-Solihat, M.K.; Nahon, M. Flexible Multibody Dynamic Modeling of a Floating Wind Turbine. *Int. J. Mech. Sci.* **2018**, *142–143*, 518–529. [CrossRef]
39. Xu, J.; Zhang, L.; Li, X.; Li, S.; Yang, K. A Study of Dynamic Response of a Wind Turbine Blade Based on the Multi-Body Dynamics Method. *Renew. Energy* **2020**, *155*, 358–368. [CrossRef]
40. Tarfaoui, M.; Nachtane, M.; Boudounit, H. Finite Element Analysis of Composite Offshore Wind Turbine Blades Under Operating Conditions. *J. Therm. Sci. Eng. Appl.* **2019**, *12*, 011001. [CrossRef]

41. Boudounit, H.; Tarfaoui, M.; Saifaoui, D.; Nachtane, M. Structural Analysis of Offshore Wind Turbine Blades Using Finite Element Method. *Wind Eng.* **2020**, *44*, 168–180. [CrossRef]
42. Spalart, P.; Allmaras, S. A One-Equation Turbulence Model for Aerodynamic Flows. In Proceedings of the 30th Aerospace Sciences Meeting and Exhibit, Reno, NV, USA, 6–9 January 1992; Aerospace Sciences Meetings. American Institute of Aeronautics and Astronautics: Reston, VA, USA, 1992.
43. Bechmann, A.; Sørensen, N.N.; Zahle, F. CFD Simulations of the MEXICO Rotor. *Wind Energy* **2011**, *14*, 677–689. [CrossRef]